Supercapacitor Performance of Perovskite La$_{1-x}$Sr$_x$MnO$_3$

Xueqin Lang[a], Haiyang Mo[b], Xiaoying Hu[b, *]Hongwei Tian[a, *]

[a] Key Laboratory of Automobile Materials of MOE and Department of Materials Science, Jilin University, Changchun, 130012, China;

[b]College of Science, Changchun University, Changchun, 130022, China;

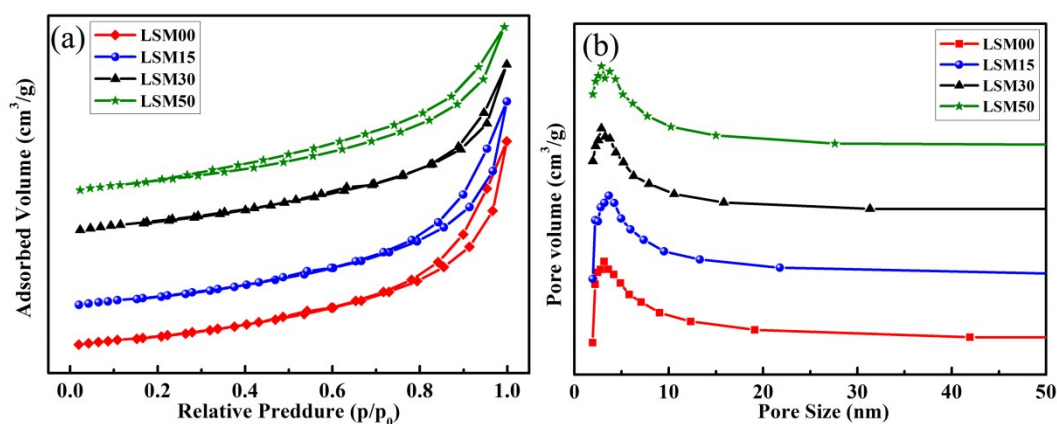* Correspondence: E-mail: tianhw@jlu.edu.cn (H.W. Tian); huxy@ccu.edu.cn (X.Y. Hu)

Fig.S1. (a) N$_2$ sorption isotherms and (b) pore size distributions of the LSM powders.

From Fig.S1a, it can be seen that the N$_2$ adsorption isotherms presented type III isotherms having uniform hysteresis loop in the large pressure range of 0-1 p/p$_0$. It is observed that most of the pores for LSM fall into the size range of 2 to 10 nm, which composed of nanoparticles. (Fig.S1b)
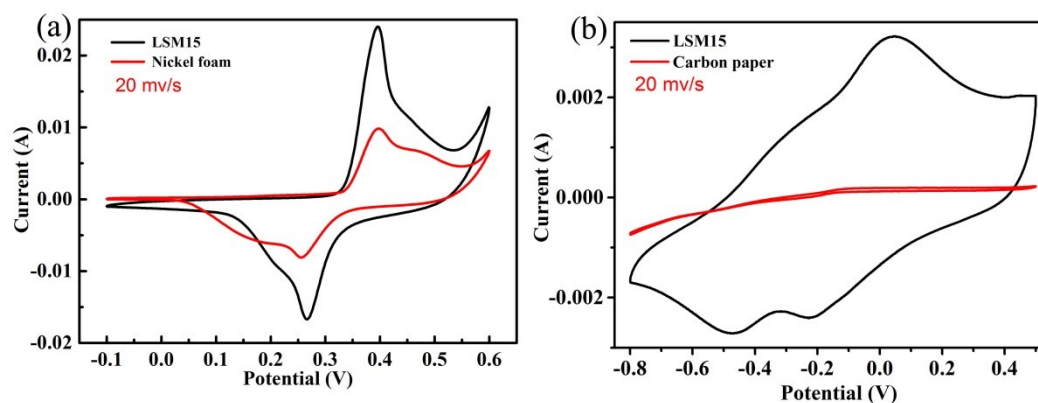

Fig.S2. The cyclic voltammetry (CV) curves of (a) nickel foam and nickel foam-LSM15 electrodes; (b) carbon paper and carbon paper-LSM15 electrodes measured at a scan rate 20 mV·s^{-1} in 1 M KOH solution.

In this study, we first studied the effect of collector on electrode materials using nickel foam and carbon paper as collector, because the porous substrates can improve performance, which, by providing electrolyte channels through the electrode that maximize contract with the active material, can enhance the charge transfer process. Through the experiment, we found that the electrode material loaded on the nickel foam, the electrochemical performance can be significantly improved by the interaction between active material and current collector, as can be seen in Fig.S2a. At scanning rate of 20 mV·s^{-1}, the specific capacitance of nickel

foam–LSM15 electrode is 235 F·g^{-1} while the net capacitance comes from LSM15 is 98 F·g^{-1}. The contribution of the nickel foam current collector is greater than that of the LSM15 active material, which is not conducive to the study of the redox reaction of the active substance itself. From the CVs of carbon paper and carbon paper-LSM15 in Fig.S2b, it can be seen that the carbon paper has a very small CV area, indicating that the contribution of carbon to capacitance can be ignored. The specific capacitance of carbon paper–LSM15 electrode is 62.3 F·g^{-1} at scanning rate of 20 mV·s^{-1}, LSM15 plays the most important role. Therefore, carbon paper for the substrate is conducive to our full study of electrode materials.
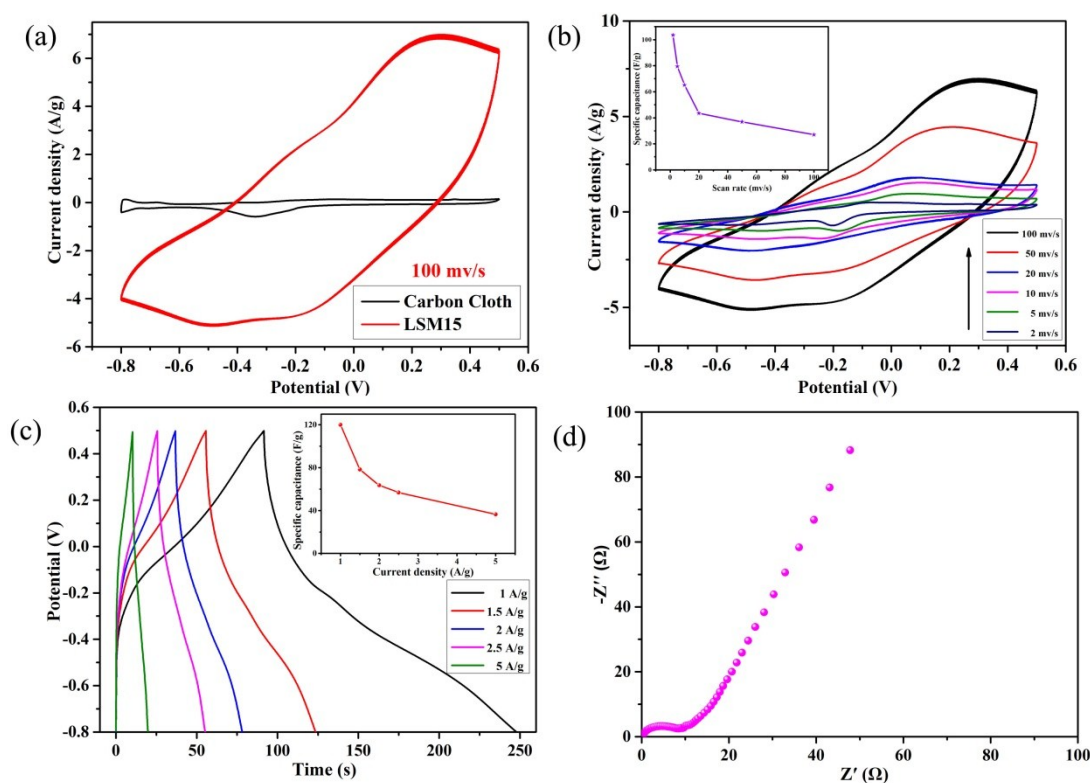
Fig.S3. (a) Comparation of CV curves of carbon cloth and LSM15 loaded on carbon cloth at scan rate of 100 mv/s in 1 M KOH aqueous solutions;(b) the CVs at different scan rates and corresponding specific versus scan rates of LSM15 on carbon cloth;(c) the GCDs of LSM15 on carbon cloth and specific capacitance at different current densities; (d) Nyquist plots of LSM15 loaded on carbon cloth.

To meet the demand of portable, flexible and wearable electronic devices, many attempts have been devoted to developing flexible supercapacitor. Li et al. reported they have successfully converted a commercial cotton T-shirt into activated carbon textiles (ACTs) with highly conductivity and flexibility for flexible energy storage application.[1] In order to demonstrate the feasibility of LSM in flexible supercapacitors, we loaded the active material LSM15 onto the carbon cloth. As shown in Fig.S3a, compared to LSM15, the carbon cloth has a smaller CV area, and the contribution of the specific capacitance can be neglected. The electrochemical properties of the LSM15 electrode materials are more elucidated by CV in a 1 M KOH solution in the range between -0.8 and 0.5 V at different potential scan rates ranging from 2 to 100 mV·s^{-1}. (Fig.S3b) The CVs for the electrode exhibits distinct redox peaks due to the intercalation/deintercalation of OH$^-$ into/from LSM15 lattice accompanied by the electrochemical conversion between Mn^{2+}/Mn^{3+} and Mn^{3+}/Mn^{4+}. With the scan rates increase, the specific capacitance decreases. The corresponding specific

capacitances at the scanning rates of 2, 5, 10, 20, 50 and 100 mV·s^{-1} are 103.5, 79.5, 65.2, 43.5, 36.9 and 27 F·g^{-1}, respectively. It is apparent that the discharge time is longer than charge times, exhibiting a super high coulombic efficiency, higher than 100%. The specific capacitance values calculated from the discharge curves for LSM15 materials are 120, 78.3, 63.6, 56.8 and 36.5 F·g^{-1} respectively at current density of 1, 1.5, 2, 2.5 and 5 A·g^{-1} shown in Fig.S3c. From the EIS test, the small R$_{ct}$ indicates good electron transport path and easy ion accessibility. In addition, the straight-line display at low frequencies shows a slope close to 90°, indicating improved conductivity and low ionic diffusion resistance (Fig.S3d). LSM15 has good electrochemical properties on flexible substrates and is expected to be applied to flexible devices and wearable electronic products in the future.
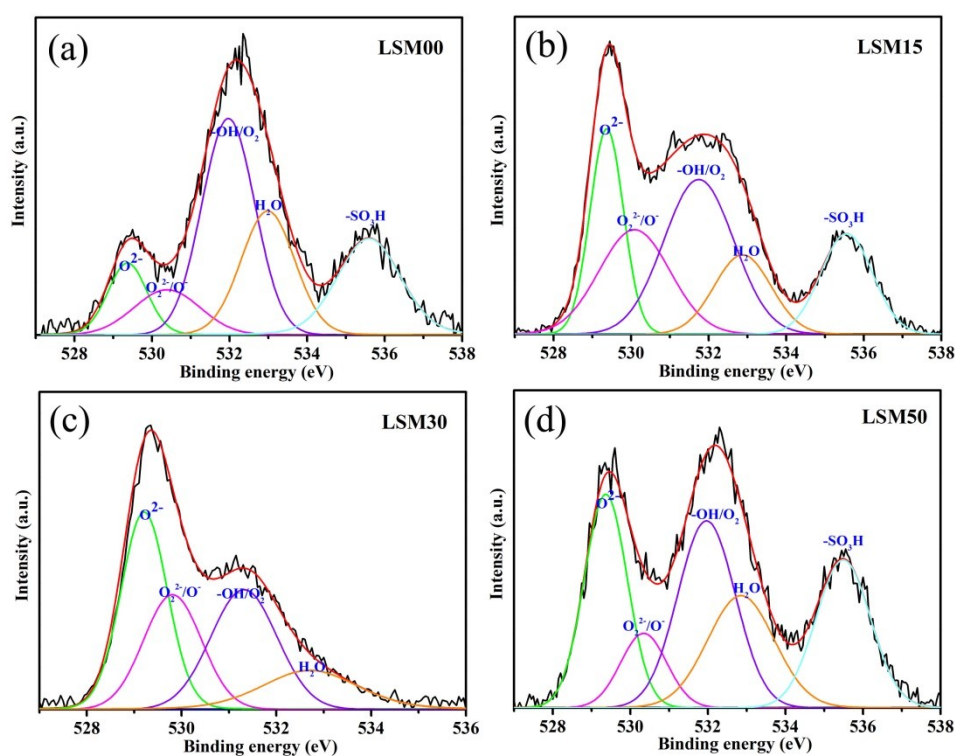
Fig.S4. The O1s XPS spectra of (a) LSM00, (b) LSM15, (c) LSM30 and (d) LSM50.

The O1s spectrum of LSM can be deconvoluted into four characteristic peaks: lattice oxygen species (O^{2-}) highly oxidative oxygen species (O_2^{2-}/O^-), hydroxy groups (-OH) or surface-adsorbed O^2, and surface-adsorbed H_2O, as shown in Fig.S4. The –SO$_3$H groups comes from the binder of nafion. The atomic percentages of oxygen-related sites in different chemical states were expressed as area of one state of oxygen peak to the total oxygen area, indicating that the concentration of oxygen vacancies in the material for qualitative analysis. The relative concentrations of different oxygen species from LSM were shown in the Table S1. The amount of O$_{ads}$ (O_2^{2-}/O^-) is intimately associated with the oxygen vacancy density of perovskite. Along with Sr-doping growth, it is notable that the adsorption oxygen increases first and then decreases with the increase of strontium content, and has the most oxygen vacancies when strontium content is 15%.

Table S1. O1s XPS peak deconvolution results of LSM00, LSM15, LSM30 and LSM50.

Sample	O^{2-} (%)	O_2^{2-}/O^- (%)	$-OH/O_2$ (%)	H_2O (%)
LSM00	12.7	12.4	47.9	28.3
LSM15	23	25	37	15
LSM30	33.4	23.7	28.4	14.5
LSM50	29.8	11	34.7	24.5

Table S2. The specific capacitance of LSM electrode materials at different scan rates.

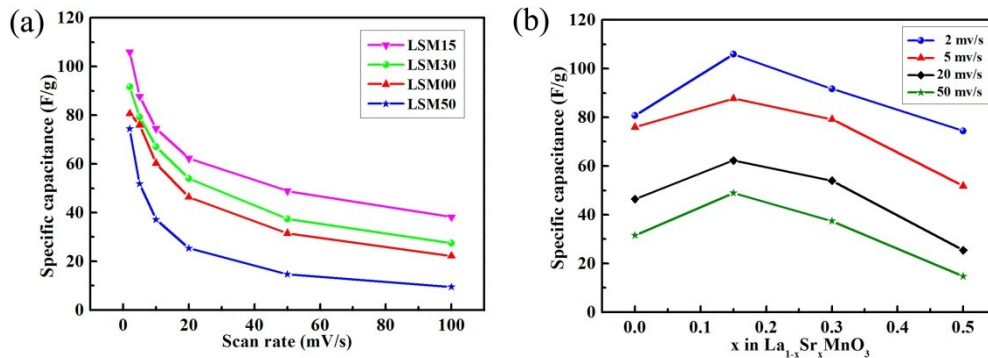| materials	2mv/s (F/g)	5mv/s (F/g)	10mv/s (F/g)	20mv/s (F/g)	50mv/s (F/g)	100mv/s (F/g)
LSM00	80.7	76.0	60.3	46.4	31.5	22.2
LSM15	105.9	87.7	74.5	62.3	48.9	38.2
LSM30	91.7	79.2	67.0	54.0	37.4	27.5
LSM50	74.4	51.8	37.2	25.4	14.7	9.5

Fig.S5. (a) The specific capacitance at different scan rates; (b) the variation between capacitance and the ratio of x in $La_{1-x}Sr_xMnO_3$ for four electrodes at scan rate of 2, 5, 20 and 50 mV·s⁻¹.

Table 2 shows the specific capacitance of LSM at different scan rates in 1 M KOH electrolyte. It is reported that the specific capacitance of $(La_{0.75}Sr_{0.25})_{0.95}MnO_{3-\delta}$ reaches 56 F·g⁻¹ at scan rate of 2 mV·s⁻¹. [2] By adjusting the amount of strontium doped, the specific capacitance of LSM15, LSM30, LSM00 and LSM50 electrode is 105.9, 91.7, 80.7 and 74.4 F·g⁻¹ at 2 mV·s⁻¹ in 1 M KOH electrolyte, respectively. As shown in Fig.S5a, the specific capacitance of LSM electrode materials decreased while the scan rate increasing, from high to low is: LSM15, LSM30, LSM00 and LSM50.The reason for the low scan rate with high specific capacitance is due to the fact that the high concentration of OH⁻ can sufficiently reach the active site and the redox reaction is carried out more completely. A higher scan rate causes the depletion or saturation of protons in the electrolyte within the electrode materials during the redox process, and only the external surface of electrode materials can be used for energy storage, resulting in low specific capacitance at high scan rates[3]. The variation of the specific capacitance with Sr doping ratio at different sweep rates is presented in Fig.S5b. In the scan rates range of 2, 5, 20 and 50 mV·s⁻¹, the maximum specific capacitance occurs when the doping amount is 15%, followed by 30%. While doping 50%, the overall performance is degraded due to serious lattice distortion.
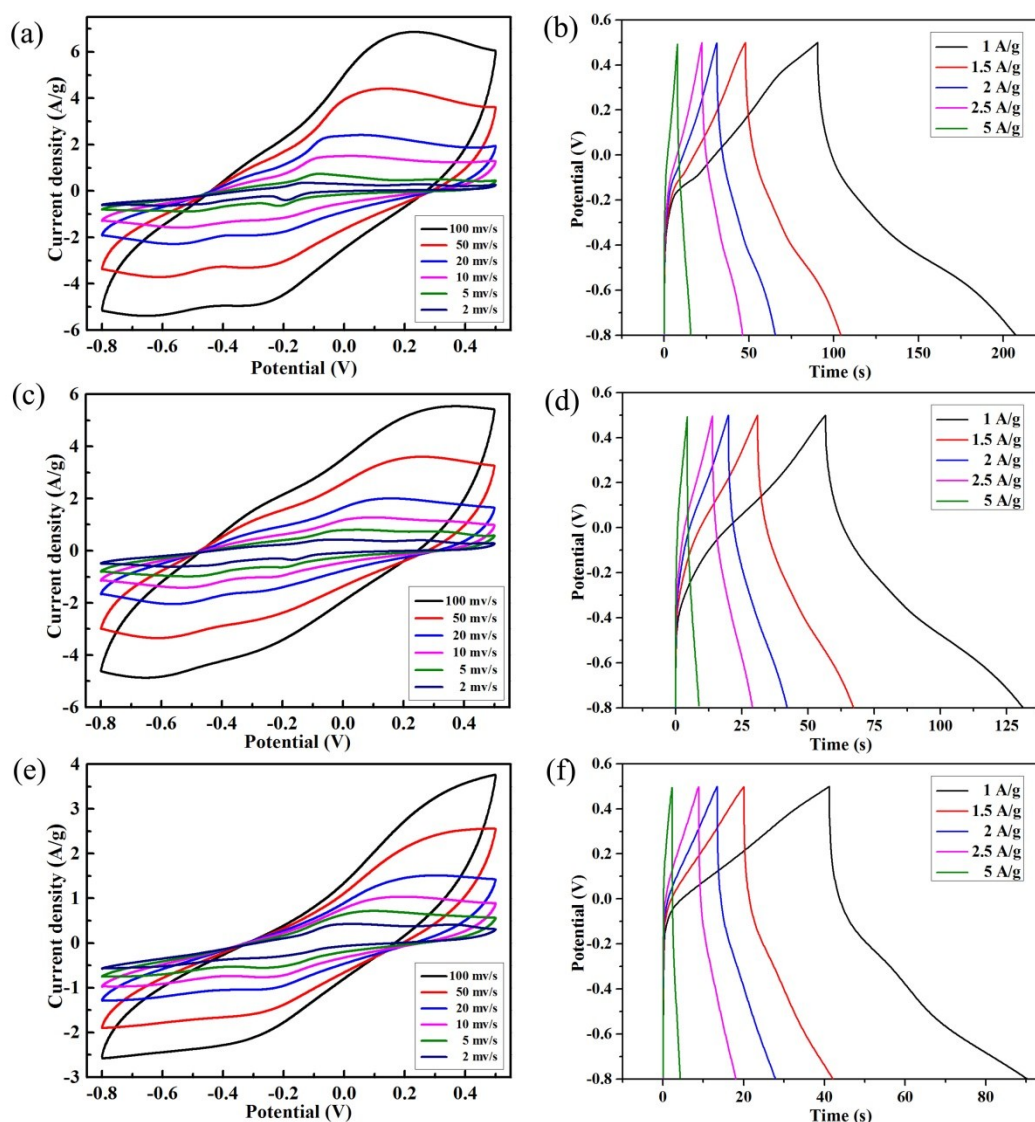
Fig.S6. The CV curves of LSM30, LSM00 and LSM50 electrode materials at different scan rates corresponding to (a), (c) and (e); the GCD curves for (b) LSM30, (d) LSM00 and (f) LSM50 electrode materials at different current densities in 1 M KOH aqueous solution.

In the Fig.S6 (a, c, e), the CV curves of LSM30, LSM00 and LSM50 electrode materials at various scan rates were characterized by a standard three-electrode configuration in 1 M KOH aqueous solution. The stable CV Curves with remarkable redox peak indicated that the specific capacitance is attributed to the apparent pseudo-capacitance as the scan rate increased from 2 to 100 mV·s^{-1}. The peak is due to the oxygen vacancy being filled with the oxidation of local Mn^{2+} ions to Mn^{3+} and then to Mn^{4+}. Additionally, the CV curve shape of the electrode material is still stable when the scanning speed increases, suggesting good reversibility, it can be also proved by symmetrical CP curves, as shown in Fig.S6 (b, d, f), it can be seen that the asymmetry shapes of the charge-discharge curves in the whole range of electric potential reflect a typical pseudocapacitor behavior. Because no phase transition happened during the O^{2-} intercalation or extraction process, the

GCD curves did not show the platform that was typical for a two phase electrode reaction process. It is obvious that the charging and discharging time at 1 A·g^{-1} is the longest.

1.   L. Bao and X. Li, *Adv Mater*, 2012, **24**, 3246-3252.
2.   J. Lü, Y. Zhang, Z. Lü, X. Huang, Z. Wang, X. Zhu and B. Wei, *RSC Advances*, 2015, **5**, 5858-5862.
3.   K. Wang, Z. Zhang, X. Shi, H. Wang, Y. Lu and X. Ma, *RSC Advances*, 2015, **5**, 1943-1948.